Multidecadal Changes in the Vertical Temperature Structure of the Tropical Troposphere

Dian J. Gaffen,[1]* Benjamin D. Santer,[2] James S. Boyle,[2] John R. Christy,[3] Nicholas E. Graham,[4] Rebecca J. Ross[1]

Trends in global lower tropospheric temperature derived from satellite observations since 1979 show less warming than trends based on surface meteorological observations. Independent radiosonde observations of surface and tropospheric temperatures confirm that, since 1979, there has been greater warming at the surface than aloft in the tropics. Associated lapse-rate changes show a decrease in the static stability of the atmosphere, which exceeds unforced static stability variations in climate simulations with state-of-the-art coupled ocean-atmosphere models. The differential temperature trends and lapse-rate changes seen during the satellite era are not sustained back to 1960.

Satellite observations of global atmospheric temperatures by the microwave sounding unit (MSU) (*1*) exhibit little or no trend (or a slight cooling) in deep-layer mean tropospheric temperature during 1979–97 (*2*). Over the same period, conventional, in situ meteorological observations suggest that globally averaged surface air temperature increased at a rate of ~0.1 to 0.2 K decade^{-1} (*3, 4*). This difference has been attributed to problems with the satellite record (*5–7*), biases in the surface observations (*3, 8*), or the large statistical uncertainty of the two linear trend estimates based on short data records (*9–11*). Recent adjustments to the MSU data (*2, 6*) only partially resolve the discrepancy by removing an artificial cooling trend, attributable to decreases in satellite orbital heights, in the lower tropospheric temperature estimates (MSU 2LT) relative to both the mid troposphere [MSU channel 2 (MSU 2)] and the surface (*12*).

Another possible explanation for the different trends is that surface and lower tropospheric temperatures may respond differently to changes in a suite of natural and human-induced climate forcings, including well-mixed greenhouse gases, stratospheric and tropospheric ozone, tropospheric aerosols, and stratospheric volcanic aerosols (*7, 13–15*). The debate regarding interpretation of temperature-trend differences between MSU 2LT and surface data has focused on the tropical belt, where the discrepancy is largest (*2, 5, 16*). Here, we investigate the existence and possible interpretation of differential temperature trends. We present a third, independent set of observations, from radiosondes (weather balloons) (*17*), supporting the finding of greater tropical warming near the surface than in the lower troposphere during the MSU period. The data also yield direct estimates of changes in both the vertical temperature profile (or lapse rate) and the height of the freezing level of the tropical atmosphere, both of which corroborate the differential temperature trends. In addition, they show the multidecadal variability of temperature, freezing level, and lapse rate since 1960 (*18*).

Radiosondes offer a distinct advantage over MSU data in assessing changes in the vertical structure of atmospheric temperature, because they measure continuously as they ascend from the surface to the lower stratosphere. Each sounding is produced by a new instrument, so spurious trends due to long-term instrumental drift are not a concern. Instrument changes over time could introduce artificial trends. Quantifying these effects is difficult, but the problem is much less serious in the lower troposphere than at higher altitudes (*19*). Soundings include temperature observations at the surface and at the 700- and 500-hPa levels (~3200 and 5800 m above the surface in the tropics). These correspond closely to the levels of peak signal in the MSU deep-layer mean temperature retrievals; MSU 2LT and MSU 2 vertical weighting functions peak at 740 and 590 hPa, respectively (*20*).

Using quality-controlled daily or twice-daily observations from 58 long-term tropical (30°N to 30°S latitude) radiosonde stations (shown in Fig. 1), we computed temperature trends (*21*) at the surface and in the lower troposphere for both the 19-year period 1979–97 (covering that of the MSU observations) and the 38-year period beginning in 1960. During the longer period, monthly mean surface temperatures increased ~0.05 to 0.21 K decade^{-1}. [Here and below we give the range of the combined 95% confidence intervals for the 0000 and 1200 UTC estimates (Fig. 2A).] The tropical lower and mid troposphere experienced greater warming (0.11 to 0.26 K decade^{-1} at 700 hPa and 0.12 to 0.26 K decade^{-1} at 500 hPa), a pattern consistent with model projections of the vertical structure of tropospheric warming associated with increasing concentrations of well-mixed atmospheric greenhouse gases (*13, 22*). However, although the surface warmed (0.05 to 0.28 K decade^{-1}) during 1979–97, lower tropospheric temperatures experienced a small, and at many locations not statistically significant, decrease (−0.22 to +0.08 K decade^{-1} at 700 hPa and −0.26 to +0.08 K decade^{-1} at 500 hPa), as shown in Fig. 2A. Thus, these tropical radiosonde temperature data show the same pattern of surface warming and tropospheric cooling since 1979 as the independent surface and MSU observations. The difference is statistically significant despite relatively large confidence intervals on the trends at different levels (*10*).

As further evidence of different tropospheric temperature trends during the MSU period and the longer period, Fig. 2B shows trends in the height of the tropical freezing level based on the same radiosonde data set used above. The

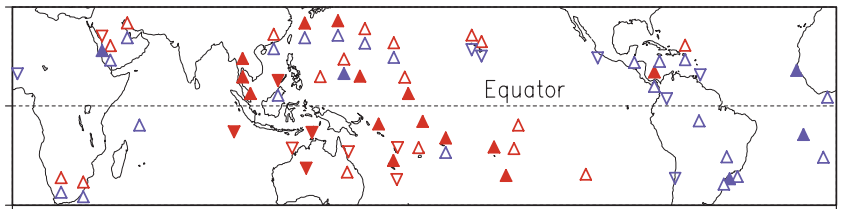

Fig. 1. Tropical radiosonde station network and 1979–97 lapse-rate trends. Sign and statistical significance of trends (*21*) in surface-to-700-hPa lapse-rate anomalies (*29*) at individual radiosonde stations during 1979–97. Trends based on 0000 and 1200 UTC observations, in red and blue, respectively, show the different spatial sampling at the two standard observation times, which results from many stations making only one observation daily, usually during daylight. Triangles with apex up or down indicate increases or decreases in lapse rate, respectively; solid triangles indicate trends that are significantly different from zero at the 95% confidence level (*10*).

[1]Air Resources Laboratory, National Oceanic and Atmospheric Administration, R/ARL, 1315 East-West Highway, Silver Spring, MD 20910, USA. [2]Program for Climate Model Diagnostics and Intercomparison, Lawrence Livermore National Laboratory, Livermore, CA 94550, USA. [3]Earth System Science Laboratory, University of Alabama–Huntsville, Huntsville, AL 35899, USA. [4]Climate Research Division, Scripps Institution of Oceanography, La Jolla, CA 92093, USA.

*To whom correspondence should be addressed. E-mail: dian.gaffen@noaa.gov

freezing level is typically at 4.5 to 5.0 km, or 550 to 600 hPa. Using radiosonde data similar to those used here, Diaz and Graham (*23*) noted significant upward trends in the tropical freezing level during 1970–86. They linked the retreat of tropical mountain glaciers to these trends and, on the basis of close agreement between observed trends and those simulated by versions of the European Centre/Hamburg (ECHAM) (*24*) atmospheric general circulation model, further suggested that the freezing-level trends were driven by an enhanced hydrologic cycle and increasing tropical sea surface temperatures (SSTs).

Interannual variations in freezing level are far better correlated with mid tropospheric temperature than with surface air temperature (*25*), so it is not surprising that the freezing level rose ~30 m decade^{-1} during 1960–97 but lowered during the MSU period (Figs. 2B and 3C), despite comparable surface warming during the two periods (Fig. 2A). This difference in the freezing-level trend during the two periods is partly due to an upward shift in the late 1970s, before the launch of the MSU in 1979, followed by a more gradual lowering during the MSU period.

Tropical glaciers at 5- to 7-km elevation have rapidly retreated during the 1980s and 1990s (*26*), while freezing levels have lowered. This apparent incongruity might be related to (i) differences between temperature and temperature trends at these high elevations and those in the free atmosphere (*27*); (ii) changes in hydrology (*26*), rather than temperature, dominating glacial retreat; or (iii) lag in the response of glaciers to temperature changes.

In the troposphere, temperature generally decreases upward from the surface. The rate of temperature decrease with height, or lapse rate, is a measure of the static stability of the atmosphere: larger lapse rates are associated with convectively unstable situations, whereas isothermal layers (lapse rate equal to zero) and inversions (negative lapse rates) are highly stable. Average lapse rates in the tropics tend toward the moist-adiabatic value, which varies with atmospheric temperature (*28*); we find typical lapse-rate values of ~5.5 K km^{-1} for both the surface-to-700-hPa and the 700-to-500-hPa layers (*29*).

Lower and mid tropospheric lapse rates involve differences in temperature between two levels with similar interannual variations. Therefore, the interannual variability of lapse rates is much smaller than that of temperature at a single level, facilitating identification of small trends in the presence of large year-to-year variability of temperature that is common to both levels (*10*). Lapse rates in the surface-to-700-hPa layer show highly statistically significant increases (Fig. 2C), of ~0.04 to 0.13 K km^{-1} decade^{-1} during 1979–97, that are of consistent sign over most of the tropical domain (*30*) (Fig. 1). We find similar trends toward slightly greater instability (*31*) using both 0000 UTC (trend = 0.064 ± 0.028 K km^{-1} decade^{-1}) and 1200 UTC observations (trend = 0.084 ± 0.038 K km^{-1} decade^{-1}) (Fig. 3A) with different spatial sampling (Fig. 1).

We have examined lapse-rate trends based not only on monthly mean data but also on monthly extremes [25th- and 75th-percentile values (*29*)] and find that, although both extremes are becoming more unstable during the satellite era, trends in the more stable days (25th percentile) are larger than trends in the less stable days (75th percentile) (Fig. 2C). This small nonuniform shift in the frequency distribution of tropical static stability is not surprising because less stable lapse rates are more likely to lead to convective overturning (*28*).

Positive trends in 700-to-500-hPa lapse rates suggest a warming of the 700-hPa level relative to the 500-hPa level during the MSU period, although the trends are not significantly different from zero (Fig. 2C). This would be consistent with MSU 2LT trends exceeding MSU 2 trends, but the MSU data in the tropical belt show the opposite (*2*), indicating some

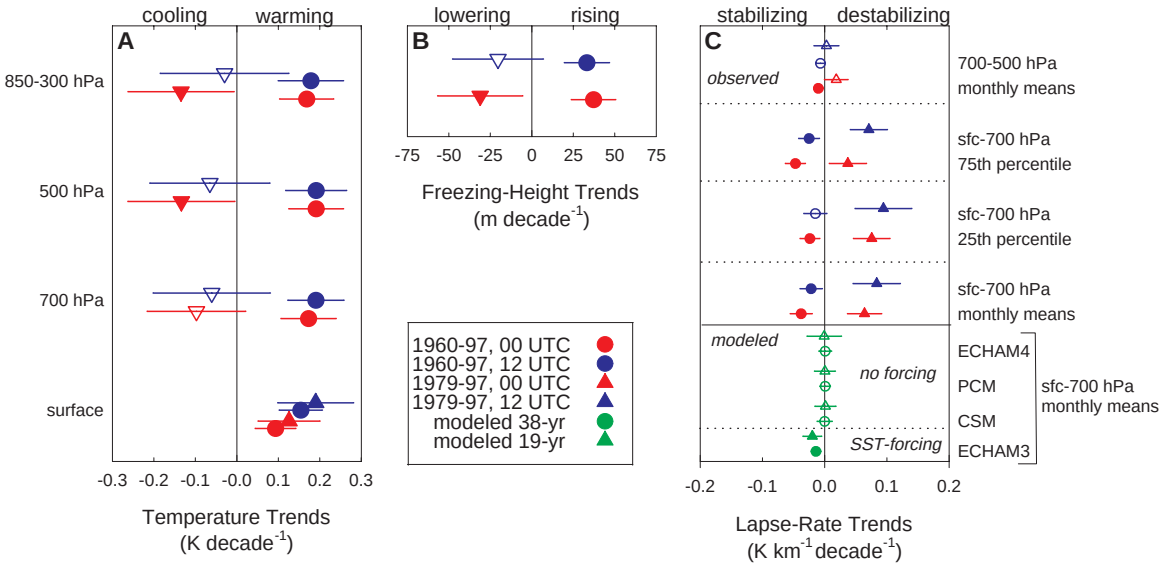

Fig. 2. Trends in temperature, freezing level, and lapse rate. (**A**) Trends in tropical average monthly temperature anomalies and confidence intervals for 1960–97 (circles) and 1979–97 (triangles). Solid symbols indicate trends significantly different from zero at the 95% confidence level, and triangles with apex up or down indicate upward or downward trends, respectively. Trends based on 0000 and 1200 UTC observations are shown in red and blue, respectively. Trends at the surface, 700-hPa, and 500-hPa levels are based on daily radiosonde temperature observations. Trends in the 850-to-300-hPa layer are based on daily layer-mean virtual temperatures computed from radiosonde geopotential height observations and are presented for comparison with the results of Angell (*11*). The same sampling criteria (*17*) were applied separately for each period of record, resulting in different station networks for the two periods. Spatial averages for 1960–97 are based on 29 stations (25 for 0000 UTC and 13 for 1200 UTC), and average daily sampling for the network was 86%. Averages for 1979–97 are based on 58 stations (41 for 0000 UTC and 34 for 1200 UTC), and average daily sampling was 90%. (**B**) Trends in tropical average height of the freezing level for the same periods as in (A). The height of the first 0°C level, either reported or interpolated between reported data levels, was identified in each sounding, as in (*23*). Trends in freezing-level pressure (not shown) are consistent with height trends. (**C**) Trends in tropical average monthly lapse-rate anomalies for the same periods as in (A). Trends shown are based on surface-to-700-hPa and 700-to-500-hPa monthly means for each station (and monthly percentiles) for comparison of trends for the most stable days (25th percentile) and the most unstable days (75th percentile). Trends in vertical temperature differences [($T_{sfc} - T_{700}$) and ($T_{700} - T_{500}$), not shown] are consistent with the lapse-rate trends and suggest that the latter are dominated by changes in temperature differences rather than changes in layer thickness. Unforced model results (shown in green) are from the sampling distributions of 19- and 38-year trends from a 300-year simulation of three coupled ocean-atmosphere climate models (*34*) with no climate forcings. The SST-forced trends are based on the average of a 10-member ensemble of simulated time series from the ECHAM3 model (*23, 24*) for the same years as the observations. All model results are based on sampling at the locations of the radiosonde stations that we used for each observational data period.

remaining observational uncertainty, perhaps related to the stratospheric influence on MSU 2. Stratospheric warming following the Mount Pinatubo eruption in 1991 may have contributed to warming in MSU 2 data relative to the 500-hPa radiosonde data used here.

These lapse-rate trends are not sustained back in time. Both surface-to-700-hPa and 700-to-500-hPa lapse rates decreased during the longer data period 1960–97 (Fig. 2C), with most of the decrease occurring during the first half of this period (Fig. 3, A and B). The decrease is larger for the most unstable days (75th percentile) than for the most stable days (Fig. 2C). Thus, temperature and lapse-rate trends during the MSU period are qualitatively different from the preceding two decades.

Contemporary coupled ocean-atmosphere global climate models have been used to simulate the unforced variability of the climate system (*5, 32*). Analysis of three state-of-the art models by Santer *et al.* (*33*) suggests that simulated global surface temperature trends over 20-year periods never exceed lower tropospheric trends by as much as the observed 0.1 K decade^{-1} for 1979–98. Neither are such trend differences simulated in these models when forced by changing atmospheric greenhouse gas and sulfate aerosol concentrations. Including the effects of stratospheric ozone depletion and the injection of aerosols into the stratosphere by the 1991 eruption of Mount Pinatubo brings the simulated trend differences closer to, but still smaller than, those observed (*14, 15, 33*).

Extending the Santer *et al.* (*33*) analysis to tropical lapse-rate changes, we have computed the distributions of 19- and 38-year trends in tropical lapse rates from unforced 300-year simulations by three climate models (*34*). The range of trends varies slightly among the models, but the observed 1979–97 lapse-rate trend is well above each of the modeled 19-year trend ranges (Fig. 2C). The modeled 38-year trend ranges overlap the confidence interval of the observed 1960–97 trend for 1200 UTC but not for 0000 UTC (Fig. 2C).

If these models are accurately characterizing the unforced decadal variability of tropical tropospheric lapse rates, then we can conclude that the observed trends for 1979–97 are likely associated with external forcings of the climate system that result in different surface and lower tropospheric temperature changes. An ensemble of simulations with the ECHAM3 atmospheric model (*24*), forced by observed SSTs, yields decreases in tropical lapse rates for both 1979–97 and 1960–97 (Fig. 3C). This result suggests that SST changes alone (which may reflect internal climate variability and external forcing) cannot adequately explain the vertical structure of atmospheric temperature trends seen during the MSU period and that the richer three-dimensional structure of natural and anthropogenic climate forcings may be required for more realistic simulations. Given uncertainties in the observations, in reconstructing the historical climate forcings (*14*), and in the climate system's response to those forcings, we may never have a complete understanding of the complex behavior of tropical tropospheric temperatures, lapse rates, and freezing levels during the past few decades. Nevertheless, the radiosonde results presented here serve to confirm, at least for the tropical regions, enhanced warming of the surface relative to the lower troposphere, as seen in satellite and surface temperature data.

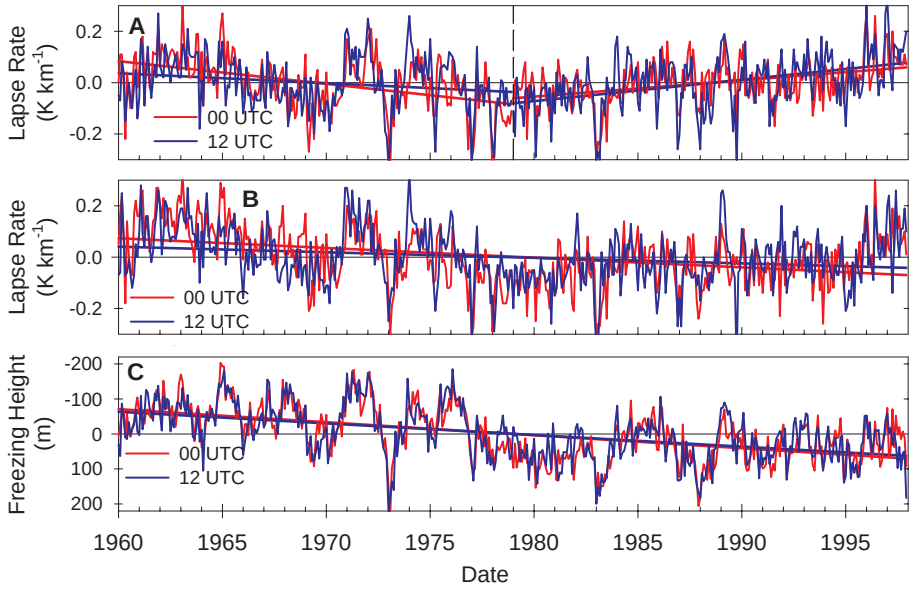

Fig. 3. Tropical average lapse-rate and freezing-level changes. (**A**) Tropical mean monthly anomalies of surface-to-700-hPa lapse rate at 0000 and 1200 UTC, shown in red and blue, respectively, for two periods of record. Different station networks for each period (31 stations for 1960–78 and 58 stations for 1979–97) maximize spatial sampling using a consistent set of data requirements (*17*). (**B**) Same as (A), but with the same 29 stations (25 for 0000 UTC and 13 for 1200 UTC) for the complete period 1960–97. (**C**) Tropical mean monthly anomalies of freezing-level height at 0000 and 1200 UTC, shown in red and blue, respectively, with the same 29 stations as in (B). The vertical axis is inverted to facilitate comparison with (A) and (B).

References and Notes

1. R. W. Spencer and J. R. Christy, *Science* **247**, 1558 (1990).
2. Trends in globally averaged temperatures for the most recent version (d) of the MSU data for the period 1979–97 are −0.04 K decade^{-1} for the mid troposphere (MSU 2) and −0.01 K decade^{-1} for the lower troposphere (MSU 2LT). The previous version (c) yields trends of +0.01 K decade^{-1} (MSU 2) and −0.04 K decade^{-1} (MSU 2LT). Trends for the tropical belt (30°N to 30°S) are −0.01 K decade^{-1} (MSU 2) and −0.07 K decade^{-1} (MSU 2LT) for version d, and +0.03 K decade^{-1} (MSU 2) and −0.10 K decade^{-1} (MSU 2LT) for version c. The two versions differ in that d includes adjustments for satellite orbital decay (*6*), diurnal sampling drift, and instrument-body temperature effects, as discussed by J. R. Christy, R. W. Spencer, and W. D. Braswell [*J. Atmos. Oceanic Tech.*, in press]. The studies cited in (*6*), (*7*), (*14*), and (*16*) use version c, or an earlier version, of the MSU data.
3. P. D. Jones, M. New, D. E. Parker, S. Martin, I. G. Rigor, *Rev. Geophys.* **37**, 173 (1999).
4. J. Hansen, R. Ruedy, J. Glascoe, M. Sato, *J. Geophys. Res.*, **104**, 30997 (1999).
5. J. Hansen *et al.*, *Clim. Change* **30**, 103 (1995).
6. F. J. Wentz and M. Schabel, *Nature* **394**, 661 (1998).
7. J. Hurrell and K. Trenberth, *Nature* **386**, 164 (1997).
8. J. R. Christy and J. D. Goodridge, *Atmos. Environ.* **29**, 1957 (1995); J. R. Christy, R. W. Spencer, E. S. Lobl, *J. Clim.* **11**, 2016 (1998).
9. D. J. Gaffen, *Nature* **394**, 615 (1998).
10. B. D. Santer *et al.*, *J. Geophys. Res.*, in press.
11. J. K. Angell, *Geophys. Res. Lett.* **26**, 2761 (1999).
12. The adjustments identified by Wentz and Schabel (*6*) were applied to globally averaged time series of MSU data, version c. As explained in (*2*), the discrepancy remains in the newer version, d.
13. V. Ramaswamy and M. M. Bowen, *J. Geophys. Res.* **99**, 18909 (1994).
14. J. Hansen *et al.*, *J. Geophys. Res.* **102**, 25679 (1997).
15. L. Bengtsson, E. Roeckner, M. Stendel, *J. Geophys. Res.* **104**, 3865 (1999).
16. J. W. Hurrell and K. E. Trenberth, *J. Clim.* **11**, 945 (1998).
17. Satellite observations, surface meteorological observations, and radiosonde observations are the three primary sources of long-term atmospheric temperature data, and they are virtually independent. MSU data are compared with, but not calibrated to, radiosonde data. The surface temperature observations in radiosonde reports may be included in surface temperature data sets (*3, 4*), but because the surface network is much denser than the radiosonde network, radiosonde observations would have a minor impact on trends derived from surface temperature data sets. Radiosonde data used in this study are from the core network of the Comprehensive Aerological Research Data Set (CARDS). Station records were used if observations were available for at least 7 days of at least 85% of all months in the 19- or 38-year period under investigation. The CARDS product is described by R. E. Eskridge *et al.* [*Bull. Am. Meteorol. Soc.* **76**, 1759 (1995)] and T. W. R. Wallis [*J. Clim.* **11**, 272 (1998)].
18. R. Toumi, N. Hartell, and K. Bignell [*Geophys. Res. Lett.* **26**, 1751 (1999)] point out the need to understand lapse-rate changes for interpreting surface versus tropospheric temperature trends as well as trends in high-altitude surface pressure and tropical freezing-level heights.
19. D. J. Gaffen, *J. Geophys. Res.* **99**, 3667 (1994); D. J. Gaffen, M. A. Sargent, R. E. Habermann, J. R. Lanzante, *J. Clim.*, in press.
20. B. D. Santer *et al.*, *J. Geophys. Res.* **104**, 6305 (1999).

21. Trends are least squares linear regression estimates. Confidence intervals are ±2 SD of the trend estimate, with the number of degrees of freedom adjusted for lag-one autocorrelation in the monthly anomaly time series.
22. A. Kattenberg *et al.*, in *Climate Change 1995: The Science of Climate Change*, J. T. Houghton *et al.*, Eds. (Cambridge Univ. Press, Cambridge, 1996), p. 285–357.
23. H. F. Diaz and N. E. Graham, *Nature* **383**, 152 (1996).
24. E. K. Roeckner *et al.*, *Report No. 93* (Max-Planck-Institut für Meteorologie, Hamburg, Germany, 1992).
25. Web table 1 is available at www.sciencemag.org/feature/data/1046022.shl.
26. L. G. Thompson *et al.*, *Global Planet. Change* **7**, 145 (1993); L. G. Thompson, *Quat. Sci. Rev.* **19**, 19 (2000).
27. P. Molnar and K. A. Emanuel, *J. Geophys. Res.* **104**, 24265 (1999).
28. P. H. Stone and J. H. Carlson, *J. Atmos. Sci.* **36**, 415 (1979).
29. For each sounding, layer mean surface-to-700-hPa lapse rates ($-\partial T/\partial Z$) were computed as $(T_{sfc} - T_{700})/(Z_{700} - Z_{sfc})$, where temperature T is the measured value at the surface and 700 hPa, Z_{700} is the geopotential height at 700 hPa, and Z_{sfc} is the surface elevation. Daily layer mean 700-to-500-hPa lapse rates were computed as $(T_{700} - T_{500})/(Z_{500} - Z_{700})$. Monthly means and quartiles were computed separately from 0000 and 1200 UTC soundings. Temporal increases in lapse rates mean a steepening of the rate of decrease of T with Z and a tendency toward more unstable conditions.
30. Empirical orthogonal function analysis of the data reveals strong spatial consistency of the lapse-rate trends. The dominant mode of variability, which explains 21% of the total variance, has a spatial pattern that is positive throughout the domain and a temporal structure showing an increase from 1979 to 1997.
31. D. S. Gutzler [*J. Atmos. Sci.* **53**, 2773 (1996)] found increasing instability at four tropical west Pacific radiosonde stations. Potential temperature differences between 300 and 1000 hPa increased during 1973–93 in association with increases in lower tropospheric water vapor.
32. R. J. Stouffer, G. C. Hegerl, S. F. B. Tett, *J. Clim.*, **13**, 517 (2000).
33. B. D. Santer *et al.*, *Science* **287**, 1227 (2000).
34. The three coupled ocean-atmosphere models are the Parallel Climate Model (PCM), the Climate System Model (CSM), and Max-Planck-Institut für Meteorologie ECHAM4/OPYC model. Based on the distributions of lapse-rate trend values in each model run, Fig. 2C shows the ranges, encompassing 95% of the distribution. Monthly layer mean lapse rates were computed in the same manner as the observations, but with monthly mean temperatures and heights at 700 hPa, 2-m (surface) air temperature, and the models' surface elevation. L. Bengtsson, E. Roeckner, and M. Stendel (*15*) discuss the ECHAM4 model; B. A. Boville and P. R. Gent [*J. Clim.* **11**, 1115 (1998)] describe the CSM; and the PCM is discussed by W. M. Washington *et al.* (*Clim. Dyn.*, in press).
35. We are grateful to L. Bengtsson, E. Roeckner, and M. Esch (Max-Planck-Institut für Meteorologie) for supplying the ECHAM3 model and the ECHAM4/OPYC simulations; T. Wigley [National Center for Atmospheric Research (NCAR)] for the CSM simulations; G. Meehl (NCAR) for the PCM simulations; M. Tyree (Scripps Institution of Oceanography) for performing ECHAM3 model runs; and J. Angell and M. Free (NOAA) for beneficial discussions.

5 October 1999; accepted 29 December 1999

Self-Assembling Amphiphilic Siderophores from Marine Bacteria

J. S. Martinez,[1] G. P. Zhang,[1] P. D. Holt,[1] H.-T. Jung,[2] C. J. Carrano,[3] M. G. Haygood,[4] Alison Butler[1]*

Most aerobic bacteria secrete siderophores to facilitate iron acquisition. Two families of siderophores were isolated from strains belonging to two different genera of marine bacteria. The aquachelins, from *Halomonas aquamarina* strain DS40M3, and the marinobactins, from *Marinobacter* sp. strains DS40M6 and DS40M8, each contain a unique peptidic head group that coordinates iron(III) and an appendage of one of a series of fatty acid moieties. These siderophores have low critical micelle concentrations (CMCs). In the absence of iron, the marinobactins are present as micelles at concentrations exceeding their CMC; upon addition of iron(III), the micelles undergo a spontaneous phase change to form vesicles. These observations suggest that unique iron acquisition mechanisms may have evolved in marine bacteria.

Low iron concentrations in surface seawater [typically from 20 pM to 1 nM (*1*)] limit primary production by phytoplankton in regions characterized by high concentrations of nitrate and other nutrients but low concentrations of chlorophyll (HNLC, high nitrate low chlorophyll) (*2*). In addition to phytoplankton and cyanobacteria, heterotrophic bacteria make up an important class of microorganisms in the ocean that are also limited by low iron levels in HNLC regions (*3*–*5*). Heterotrophic bacteria constitute up to half of the total particulate organic carbon in ocean waters (*4*), and in some regions, such as the subarctic Pacific, heterotrophic bacteria can even contain higher cellular concentrations of iron than phytoplankton (*5*). Heterotrophic bacteria thus compete successfully for iron against phytoplankton and cyanophytes and play a substantial role in the biogeochemical cycling of iron in the ocean. However, little is known about the molecular mechanisms used by marine bacteria, in particular, and other marine microorganisms, in general, to sequester iron. Marine bacteria are known to produce siderophores (*6*–*8*), which are low–molecular weight compounds secreted to scavenge Fe(III) from the environment and to facilitate its uptake into microbial cells. We report herein the structures and properties of a class of self-assembling amphiphilic siderophores produced by marine bacteria. Two families of siderophores, produced by two different genera of bacteria, each contain a unique peptidic head group that coordinates Fe(III) and one of a series of fatty acid tails.

Three strains, designated DS40M3, DS40M6, and DS40M8, were isolated from the same sample of ocean water, which had been collected at a depth of 40 m over the continental slope in the eastern equatorial Atlantic (*7*). The aquachelin siderophores (Fig. 1), produced by *Halomonas aquamarina* DS40M3 (Fig. 2), and the marinobactin siderophores (Fig. 1), produced by *Marinobacter* species strains DS40M6 and DS40M8 (Fig. 2), were isolated and purified from the supernatant of bacterial cultures, as previously described (*7*). The amino acid composition of the aquachelins and marinobactins, including the enantiomeric configuration, was determined with Marfey's reagent [*N*-a-(2,4-dinitro-5-fluorophenyl)-L-alaninamide] (*9*). The amino acid sequence was established by tandem mass spectrometry (Fig. 1) and confirmed by nuclear magnetic resonance (NMR) spectroscopy (*10*). The position of the D- and L-amino acids was determined from amino acid analysis of partially hydrolyzed peptide fragments generated from the native siderophore (*11*). Elucidation of the fatty acid moieties involved gas chromatography–mass spectrometry comparison to standard methyl ester derivatives, ozonolysis to establish the position of the double bond, and NMR to elucidate the configuration of the double bond (*10*). The connectivity of diaminobutyric acid and β-hydroxyaspartic acid in the marinobactin ring was determined by NMR (*10*).

The only terrestrial siderophores that bear a structural resemblance to marinobactins and aquachelins are the mycobactins and exochelins produced by mycobacteria, such as *Mycobacterium tuberculosis*, which also usually contain a fatty acid tail (*12*, *13*). The exochelins and mycobactins share a common hydrophilic core that coordinates Fe(III), but they differ in the substitution and chain length of the fatty acid. The hydrophilic exochelins, which are secreted

[1]Department of Chemistry and Biochemistry, University of California, Santa Barbara, CA 93106–9510, USA. [2]Department of Chemical Engineering, University of California, Santa Barbara, CA 93106, USA. [3]Department of Chemistry, Southwest Texas State University, San Marcos, TX 78666, USA. [4]Marine Biology Research Division, Scripps Institution of Oceanography, University of California, San Diego, La Jolla, CA 92093–0202, USA.

*To whom correspondence should be addressed. E-mail: Butler@chem.ucsb.edu